DOI: 10.1111/nyas.14794

ORIGINAL ARTICLE

ANNALS OF THE NEW YORK ACADEMY OF SCIENCES

Tight junction channels claudin-10b and claudin-15: Functional mapping of pore-lining residues

Caroline Hempel | Rita Rosenthal | Anja Fromm | Susanne M. Krug | Michael Fromm | Dorothee Günzel | Jörg Piontek

Clinical Physiology/Nutritional Medicine, Medizinische Klinik für Gastroenterologie, Infektiologie und Rheumatologie, Charité – Universitätsmedizin Berlin, Berlin, Germany

Correspondence
Jörg Piontek and Rita Rosenthal, Clinical Physiology/Nutritional Medicine, Medizinische Klinik für Gastroenterologie, Infektiologie und Rheumatologie, Charité – Universitätsmedizin Berlin, Campus Benjamin Franklin, Hindenburgdamm 30, 12203 Berlin, Germany.
Email: joerg.piontek@charite.de; rita.rosenthal@charite.de

Caroline Hempel and Rita Rosenthal shared first authorship.

Abstract

Although functional and structural models for paracellular channels formed by claudins have been reported, mechanisms regulating charge and size selectivity of these channels are unknown in detail. Here, claudin-15 and claudin-10b cation channels showing high-sequence similarity but differing channel properties were analyzed. Mutants of pore-lining residues were expressed in MDCK-C7 cells. In claudin-15, proposed ion interaction sites (D55 and E64) conserved between both claudins were neutralized. D55N and E64Q substitutions decreased ion permeabilities, and D55N/E64Q had partly additive effects. D55N increased cation dehydration capability and decreased pore diameter. Additionally, residues differing between claudin-15 and -10b close to pore center were analyzed. Claudin-10b–mimicking W63K affected neither assembly nor function of claudin-15 channels. In contrast, in claudin-10b, corresponding (claudin-15b-mimicking) K64W and K64M substitutions disturbed integration into tight junction and slightly altered relative permeabilities for differently sized monovalent cations. Removal of claudin-10b–specific negative charge (D36A substitution) was without effect. The data suggest that a common tetra-aspartate ring (D55/D56) in pore center of claudin-15/-10b channels directly attracts cations, while E64/D65 may be at least partly shielded by W63/K64. Charge at position W63/K64 affects assembly and properties for claudin-10b but not for claudin-15 channels. Our findings add to the mechanistic understanding of the determinants of paracellular cation permeability.

KEYWORDS
assembly, channel, claudin, electrophysiology, paracellular permeability, tight junction

INTRODUCTION

Claudins (Cldn) form the backbone of tight junction (TJ) strands and regulate paracellular solute and water permeability in epithelia and endothelia in a tissue-specific manner.[1,2] Loss of expression or gene mutations of many claudins lead to defined pathologies underlining their physiological relevance.[1,3,4] Electrophysiological studies revealed that many claudin family members, such as Cldn1, −3, and −5, seal the TJ for water, small ions, and larger solutes, whereas others form channels selective for small cations (Cldn2, −10b, −15, and −16/−19) or anions (Cldn10a and −17).[5] Thus, depending on the claudin expression profile in a given tissue, paracellular transport is regulated in a charge

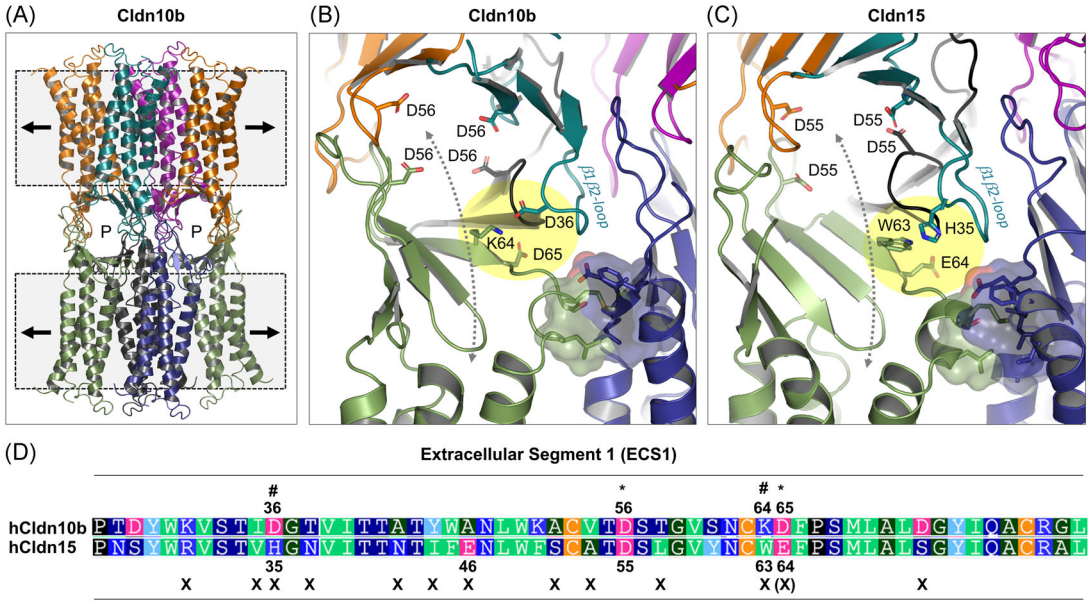

FIGURE 1 (A) Cldn10b octamer model consisting of two cohered tetrameric pores. Claudin protomers (chains) shown as colored cartoon, highlighting secondary structure elements; P indicates paracellular pores, dashed boxes indicate membranes, and arrows indicate strand extension. Channel model based on Ref. 17 and refinements (see Methods). (B) Close-up of Cldn10b pore with positions (D36, D56, K64, and D65) analyzed in this study shown as sticks. Yellow shading, close proximity of K64, D65, and D36; dashed arrow, ion path; linear *cis*-interface as transparent surface with residues as sticks; O, red; N, blue. (C) Close-up of Cldn15 pore model with positions H35, D55, W63, and E64 corresponding to those shown for Cldn10b as sticks. (D) ECS1 sequence alignment for human Cldn10b and −15. [*]Negative charges conserved between Cldn10b and −15. [#]Charged residues close to pore center and β1β2-loop differing between Cldn10b and −15 analyzed in this study. [X]Pore-lining residues differing between Cldn10b and −15. [(X)]Not differing between murine sequences

and size selective manner. Claudins are small tetraspan membrane proteins. Residues within most of the protein segments (extracellular segment [ECS] one and two, transmembrane helices, and C-terminal cytoplasmic region) have been shown to be involved in assembly of TJ strands.[2,6,25] In addition, residues within ECS1 of claudins have been shown to determine charge and size selectivity of the channels.[7–13] In particular, Cldn2 D65 and Cldn15 D55 and E64/D64 (human/mouse) were shown or indicated to determine cation selectivity.[7,11,13] Models of the architecture of TJ strands and channels formed by classic claudins have been proposed.[2] The model that is supported most by experimental data is the joined double row model based on the Cldn15 crystal structure and packing.[6,14] It has been refined for Cldn15 and other claudins in several studies, employing experimental data, molecular docking, and molecular dynamics simulations[11,15–19] (Figure 1A–C). These refined models differ in properties, such as the orientation of the ECS1 β1β2-loop missing in the original Cldn15 model,[6] other interchain interfaces, and pore diameter. Partly, this may be due to the presence of multiple interfaces enabling dynamics like lateral flexibility of TJ strands.[19,20] Molecular dynamics simulations have been also used to investigate molecular determinants of ion permeation through Cldn15 channels.[11,16] They indicated that D55 interacts with cations more strongly and contributes stronger to charge selectivity than the other negatively charged ECS1 residues E46 and E/D64.

We previously proposed a model for Cldn10b and other classic claudins,[2,21] such as Cldn15 and Cldn3, in which cis/trans-clustering of ECS1 β1β2-loops in the center between two cohered tetrameric pores is critical for assembly of channels within strands.[17] To further investigate determinants for the assembly and the function of prototypic paracellular cation channels, we compared human Cldn10b and Cldn15, the two channel-forming claudins with the highest sequences homology (67% sequence similarity, excluding C-terminal cytoplasmic part). Both form cation channels but differ in tissue expression pattern (e.g., Cldn15 in intestine, and Cldn10b in kidney and glands), alkali metal, and water permeability, as well as pore diameter.[22,23]

To analyze the molecular mechanism underlying the differing channel properties, the negatively charged residues D55 and E64 of Cldn15 that are conserved between Cldn10b and −15 (Figure 1) and indicated to be involved in charge selectivity[7,11,12] were analyzed. In addition, charged residues close to the pore center differing between Cldn10b and Cldn15 were investigated (K64/W63 and D36/H35). MDCK-C7 cells stably expressing the corresponding claudin mutants were functionally analyzed as established in previous studies.[3,22,24]

The data suggest that D55 in the center of the Cldn15 pore interacts directly with cations, whereas E64 is at least partly shielded by residues, such as W63, and affects ion permeation indirectly. Although a positive charge at position 63 does not affect Cldn15 channels, the charge at the corresponding position 64 is essential for proper assembly of Cldn10b channels. The claudin assembly is proposed to depend on the β1β2 loop. However, D36 in the β1β2 loop is neither essential for assembly nor function of Cldn10b channels.

METHODS

Plasmids

Previously published constructs of human Cldn10b and Cldn15[22,24] were used as templates for generation of Cldn10b and Cldn15 mutants. YFP-Cldn10b-wt, YFP-Cldn10b-D36A, and YFP-Cldn10b-K64M were published previously.[17] Here, the following claudin mutants were generated by two-step PCR followed by restriction cloning as described previously:[28] CFP-Cldn15-W63K and YFP-Cldn10b-K64W and 1xFLAG-Cldn15-D55N, Cldn15-E64Q, and Cldn15-D55N/E64Q. The primers used for generation of the claudin mutants are shown in Table S1. Afterward, Cldn15-wt and -W63K were subcloned into pCMV10 vector for N-terminal 3×FLAG tag using *Hind*III/*Xba*I restriction sites for cloning. Cldn10b-wt was subcloned into pCi puro using the restriction sites *Nhe*I/*Not*I. Cldn10b-D36A, -K64M, and -K64W were subcloned into pCi puro/Cldn10b-wt using *Nhe*I/*Eco*RI restriction sites for cloning. All constructs cloned into this expression vector were used for generation of stably expressing cell lines.

Cell culture and transfection

HEK293 (HEK) cells and MDCK-C7 cells were cultured in MEM-Earle's media (Sigma-Aldrich, Germany) supplemented with 10% (v/v) fetal bovine serum, 100 U/ml penicillin, and 100 μg/ml streptomycin (Sigma-Aldrich) at 37°C in a humidified 5% CO_2 atmosphere. Cell lines were transfected using polyethylenimine (HEK, Polysciences Inc., Warrington, PA, USA) or Lipofectamine 2000 (MDCK-C7; Invitrogen, Carlsbad, CA, USA) according to the manufacturer's recommendations 24 h postseeding. For stable cell lines, successfully transfected cell clones were selected using 1000 U/ml G418-BC (Biochrom, Germany) (3xFLAG-Cldn15-wt, 3xFLAG-Cldn15-W63K, CFP-Cldn15-W63K, YFP-Cldn10b-wt, YFP-Cldn10b-K64W and 1xFLAG-Cldn15-wt, Cldn15-D55N, Cldn15-E64Q, and Cldn15-D55N/E64Q) or 10 μg/ml puromycin (Cldn10b-wt, Cldn10b-D36A, Cldn10b-K64M, and Cldn10b-K64W) and maintained as clonal or polyclonal cell lines with 600 U/ml G418-BC or 1 μg/ml puromycin.

Freeze-fracture electron microscopy

Stably transfected HEK and MDCK C7 cell lines were grown until confluency, washed with PBS containing Ca^{2+}/Mg^{2+}, fixed with 2.5% glutaraldehyde (electron microscopy [EM] grade; Sigma-Aldrich) in PBS with Ca^{2+}/Mg^{2+} for 2 h, and subsequently incubated in 10% (v/v), then in 30% (v/v) glycerol, and finally frozen in liquid nitrogen-cooled Freon 22. Cells were then fractured at −100°C in a vacuum evaporator (Denton DV-502) and platinum and carbon were used for replica generation and contrasting. The resulting replicas were treated with sodium hypochloride, picked up on grids (Ted Pella Inc.), and analyzed with a video-equipped Zeiss 902A electron microscope (Carl Zeiss AG; Olympus iTEM Veleta). For morphometric analysis, magnification of 51,000× was used. Vertical grid lines were drawn at 200-nm intervals perpendicular to the most apical TJ strand, and the number of strands horizontally oriented within the main TJ meshwork was counted at intersections with grid lines. The distance between the most apical and last strand within the network was measured and defined the meshwork depth. Strand discontinuities of >20 nm were defined as "breaks," counted, and expressed as number per micrometer length of horizontally oriented strands. Strand appearance was further discriminated into "particle type" or "continuous type." The density of (bicellular) TJ strands was calculated as the number of strands/meshwork depth.

Immunoblotting

Expression levels of claudin constructs in MDCK C7 cells were determined by immunoblotting. Confluent cell layers were lysed in total lysis buffer containing 10 mM Tris (pH 7.5), 150 mM NaCl, 0.5% Triton X-100, and 0.1% SDS with EDTA-free protease inhibitor cocktail (cOmplete™ EDTA free; Roche, Germany). After centrifugation (10,000 × *g*, 4°C, 10 min), supernatant was analyzed. Protein concentrations were determined using bicinchoninic acid protein assay reagent (Pierce, San Antonio, TX, USA). Proteins (5–20 μg) were heated for 5 min at 65–95°C under reducing conditions (presence of 150 mM DTT), separated by 10–12.5% SDS-PAGE, and blotted on PVDF membrane. Proteins were probed with rabbit anti-claudin-10 or anti-claudin-15 (1:1000; Thermo Fischer Scientific, Waltham, MA, USA), mouse anti-FLAG (1:10,000; Sigma, Ronkonkoma, NY, USA) or mouse anti-β-actin for loading control (1:10,000, AC-15; Sigma). Immunodetection was performed with HRP-conjugated secondary antibodies (1:10,000; Jackson ImmunoResearch, West Grove, PA, USA) in combination with Lumi-Light or the Lumi-Light^{PLUS} Western blotting kit (Roche).

Immunostaining

Stable MDCK-C7 cell lines were grown on Millicell PCF filter supports (area 0.6 cm^2, pore diameter 0.4 μm; Millipore Merck, Germany) for 7 days, washed with PBS, including Ca^{2+}/Mg^{2+}, and fixed in 2% PFA/PBS with Ca^{2+}/Mg^{2+} (16% PFA, Electron Microscopy Sciences, Hartfield, PA, USA). Cells were permeabilized for 5 min in 0.5% Triton-X-100/DPBS, blocked (1% BSA, 0.1% Triton-X 100 or 1% BSA, 6% goat serum, 0.1% Triton-X 100) for 15 min, and subjected to rabbit anti-claudin-10 (1:200; AssayBiotech, Fremont, CA, USA) or rabbit anti-claudin-15 (1:100, Invitrogen, Karlsruhe, Germany) and mouse anti-occludin (1:200; Invitrogen, Karlsruhe) or mouse anti-ZO1 (Invitrogen, Karlsruhe) at 4°C overnight. Secondary antibodies (1:500; Alexa-Fluor 594 goat anti-mouse IgG, Alexa Fluor 488 goat anti-rabbit IgG; Jackson ImmunoResearch) plus DAPI (4′,6-diamidino-2-phenylindole dihydrochloride, 1:1000) were applied at 37°C for 60 min. Images were acquired with a confocal laser scanning microscope (LSM 780, Carl Zeiss Microscopy GmbH, Jena, Germany) using excitation wavelengths of 594, 543, 488, and 405 nm and 63× NA 1.4 objective.

Dilution potential measurements

The permeability ratio to Na^+ over that to Cl^- (P_{Na}/P_{Cl}) was determined from dilution potentials, which were measured in Ussing chambers as described before.[24] In brief, stable MDCK-C7 cells were grown to confluency on filter supports for 7 days. Inserts were mounted between two hemichambers. Cell monolayers were equilibrated in bath solution containing 119 mM NaCl, 21 mM $NaHCO_3$, 5.4 mM KCl, 1.2 mM $CaCl_2$, 1 mM $MgSO_4$, 3 mM HEPES and 10 mM D (+)-glucose, pH 7.8, and constantly gassed with 95% O_2/5% CO_2. The temperature of the bath solution was kept at 37°C. Dilution potentials were measured by switching to a modified bath solution on either the apical or basal side, in which 59.5 mM NaCl was iso-osmotically replaced either by mannitol for calculation of sodium and chloride permeability or by the chloride salts of the alkali metal ions. To determine permeabilities for organic cations, 5 ml of this solution on the apical side was exchanged with 5 ml of a solution in which NaCl was iso-osmotically replaced by mannitol. Subsequently, 5 ml of solution from the basolateral side was replaced with the solution containing the organic cation. After reaching a stable potential, the solution on the basolateral side was replaced by the original NaCl-containing perfusion solution and another organic cation could be tested in the same way. For claudin-10b, biionic potentials of organic cations were measured at room temperature. To measure biionic potentials of divalent Ca^{2+} (and Cs^+ for comparison), the experimental setup was adapted by using bicarbonate-free bath solution containing 140 mM NaCl, 5.4 mM KCl, 1.2 mM $CaCl_2$, 1 mM $MgSO_4$, 10 mM HEPES and 10 mM D (+)-glucose, pH 7.4, and gassing with 100% O_2. At all times, transepithelial voltage and transepithelial reistance (TER) were recorded. Data of apical and basal conditions were pooled. Potential differences before and after switching the solutions were corrected for liquid junction potentials and used to calculate P_X/P_{Na} as described.[24]

Structural bioinformatics and molecular modeling

The Cldn10b octamer model was generated as described previously[17] based on an experimentally refined homology model for which a Cldn15 polymer model[6] was used as the template. The octamer model introduced by Hempel *et al.*[17] was manually refined and further energy minimized using Schroedinger Bioluminate, Maestro, Biologics suite 2020−2 (Schroedinger, LLC, Germany) with the macro model module, OPLS3e force field, water solvation, the module-defined optimal minimization method, and a gradient convergence threshold of 0.05 kJ mol^{-1} $Å^{-1}$. The Cldn15 octamer homology model was generated using the Cldn10b octamer model as template and the advanced homology modeling module of Schroedinger Bioluminate, Maestro, Biologics suite 2020−2. The model was energy minimized similar as for Cldn10b. Images of the models were created with Pymol 2.5.2 (Schroedinger, LLC,).

Statistics

The results are shown as means ± SEM. Statistical analyses were performed using GraphPad Prism version 6.0 (San Diego, CA, USA). First, normality tests were performed (D'Agostino and Pearson omnibus, Shapiro–Wilk, and Kolmogorov–Smirnov tests). Data sets exhibiting normal distribution were analyzed using Student's *t*-test with posthoc Bonferroni–Sidak correction. Data sets not showing normal distribution were analyzed using the Mann–Whitney test with posthoc Bonferroni–Sidak correction. Significance levels are denoted $^{*,\#} = p < 0.05$, $^{**,\#\#,\S\S} = p < 0.01$, $^{***,\#\#\#,\S\S\S} = p < 0.001$; *n* refers to the number of experiments.

RESULTS

Cldn15-D55N, -E64Q, and -D55N/E64Q localize to TJ in MDCK-C7 cells similar to Cldn15-wt

First, we analyzed the two negatively charged residues, D55 and E64, in Cldn15 ECS1 that are conserved conjointly between no other mammalian claudins than Cldn10b and Cldn15 and that were reportedly involved in cation selectivity of Cldn15.[7,11] Here, we directly compared charge-neutralizing mutations at the two positions in Cldn15 (D55N and E64Q). Cldn15-wt, Cldn15-D55N, Cldn15-E64Q, and Cldn15-D55N/E64Q were stably expressed in tight MDCK-C7 cells lacking endogenous channel-forming claudins, and thus, providing an established cell system for overexpression studies of channel-forming claudins.[3,22,24] Confocal microscopy showed that Cldn15-D55N, -E64Q, and -D55N/E64Q colocalized in the apicolateral membrane with the TJ marker occludin, similar to Cldn15-wt (Figure 2). In addition, freeze fracture EM analysis revealed no difference in TJ ultrastructure between Cldn15-wt- and Cldn15-mutant-expressing cells (Figure S1). A previous study showed already no ultrastructural differences between vector controls and Cldn15-wt-expressing cells.[22] Thus, the mutations did neither alter integration of Cldn15 into endogenous TJs nor ultrastructure of the latter.

In Cldn15, D55N and E64Q decrease ion permeability and D55N/E64Q double substitution has additive effect

The expression of Cldn15-wt increases conductance of MDCK-C7 cell monolayers, as shown in previous studies.[22] Expression of Cldn15-D55N, -E64Q, and -D55N/E64Q induced much lower conductance than Cldn15-wt (Figure 3A). P_{Na}/P_{Cl} (measure for preference for cation or anion selectivity) was more strongly decreased by D55N/E64Q than by the single substitutions. All substitutions reduced P_{Na} strongly and P_{Cl} weakly, at least by tendency (Figure 3C).

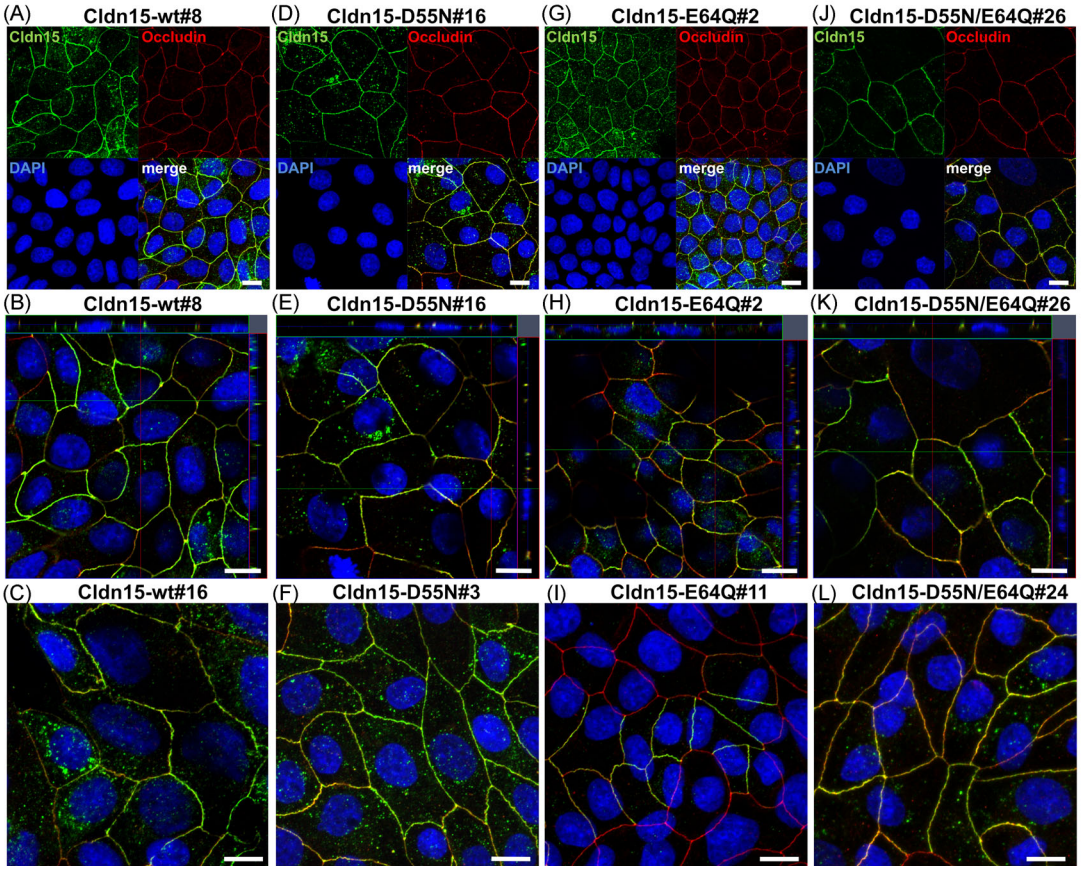

FIGURE 2 (A–L) In MDCK-C7 cells, stably expressed human Cldn15-D55N, Cldn15-E64Q, or Cldn15-D55N/E64Q localized to the TJ similar to Cldn15-wt as indicated by strong colocalization with occludin, which was used as a marker for TJ localization. Immunostaining, confocal z-stacks; bar, 10 μm; #monoclonal line number. (A, D, G, J) Maximum projection, split channels. (B, E, H, K) Orthoscopic view, merge. (C, F, I, L) Additional clones, maximum projection, merge. Cldn15-E64Q#11 showed fewer expressing cells than other clones.

These data indicated that charges of D55 and E64 are involved in ion conductance and charge selectivity of Cldn15 channels. To compare the relative permeabilities to different alkali metal ions—that is, as a measure for ion dehydration capability of the pore—biionic potentials were measured. D55N changed the Eisenman sequence drastically from I/II (P_x/P_{Na}: $Li^+ < Na^+ < K^+ = Rb^+ < Cs^+$) to X/XI ($P_x/P_{Na}$: $Cs^+ < Rb^+ < K^+ < Na^+ < Li^+$) (Figure 3D and Figure S2). A similar tendency albeit much less pronounced was observed for E64Q and D55N/E64Q (E64Q: $Cs^+ = K^+ < Na^+ < Rb^+$, $< Li^+$, no defined Eisenman sequence; D55N/E64Q#24: $Cs^+ < Rb^+ < K^+ < Li^+ < Na^+$, Eisenman sequence X; D55N/E64Q#26: $Rb^+ \leq K^+ \leq Li^+ \leq Cs^+ \leq Na^+$, no defined Eisenman sequence). For E64Q, at least P_{Li} was higher than the permeabilities for the other ions, for D55N/E64Q, P_{Li} was not lower than P_K (Figure 3D). This indicated that at least D55N increased the dehydration capability of the pore. To probe the pore diameter, permeabilities to organic cations of different sizes were measured. This indicated a smaller pore diameter for Cldn15-D55N (~5.4 Å) but not for Cldn15-E64Q (~6.1 Å) compared to Cldn15-wt (~6.1–6.4 Å) (Figure 3E,F). Here, D55N/E64Q had no uniform and at least no additive effect (~5.5–7.1 Å). For D55N/E64Q#24, the pore diameter (~7.1 Å) might be overestimated due to low sensitivity and nonlinearity of the permeability parameter (SQRT P_x/P_{Na}) caused by the low expression level and very low cation permeability for this line Figure 3C,F,G).

In sum, the data indicated that the negative charges at position 55 and 64 of Cldn15 influence conductance, cation selectivity, ion dehydration pattern, and (for D55) diameter of the pore.

Cldn15-W63K localizes to TJ similar to Cldn15-wt

Next, we analyzed residues close to the pore center differing between Cldn15 and Cldn10b, such as W63 in Cldn15 (K64 in Cldn10b). In the pore model (Figure 1), it is located between the conserved charges (Cldn15: D55 and E64; Cldn10b: D56 and D65). Most of the barrier-forming or anion channel-forming mammalian claudins contain a positively charged residue (K/R) similar to Cldn10b in this position, whereas the cation-channel Cldn2 contains a negative residue (D65). Cldn15 is the only claudin containing an aromatic tryptophan residue at this position. Thus, we generated MDCK-C7 cells stably expressing Cldn10b-like Cldn15-W63K. Confocal microscopy showed that Cldn15-W63K colocalized apicolaterally with the TJ marker ZO-1 similar to Cldn15-wt (Figure 4). Consequently, W63K did not alter the integration of Cldn15 into endogenous TJs.

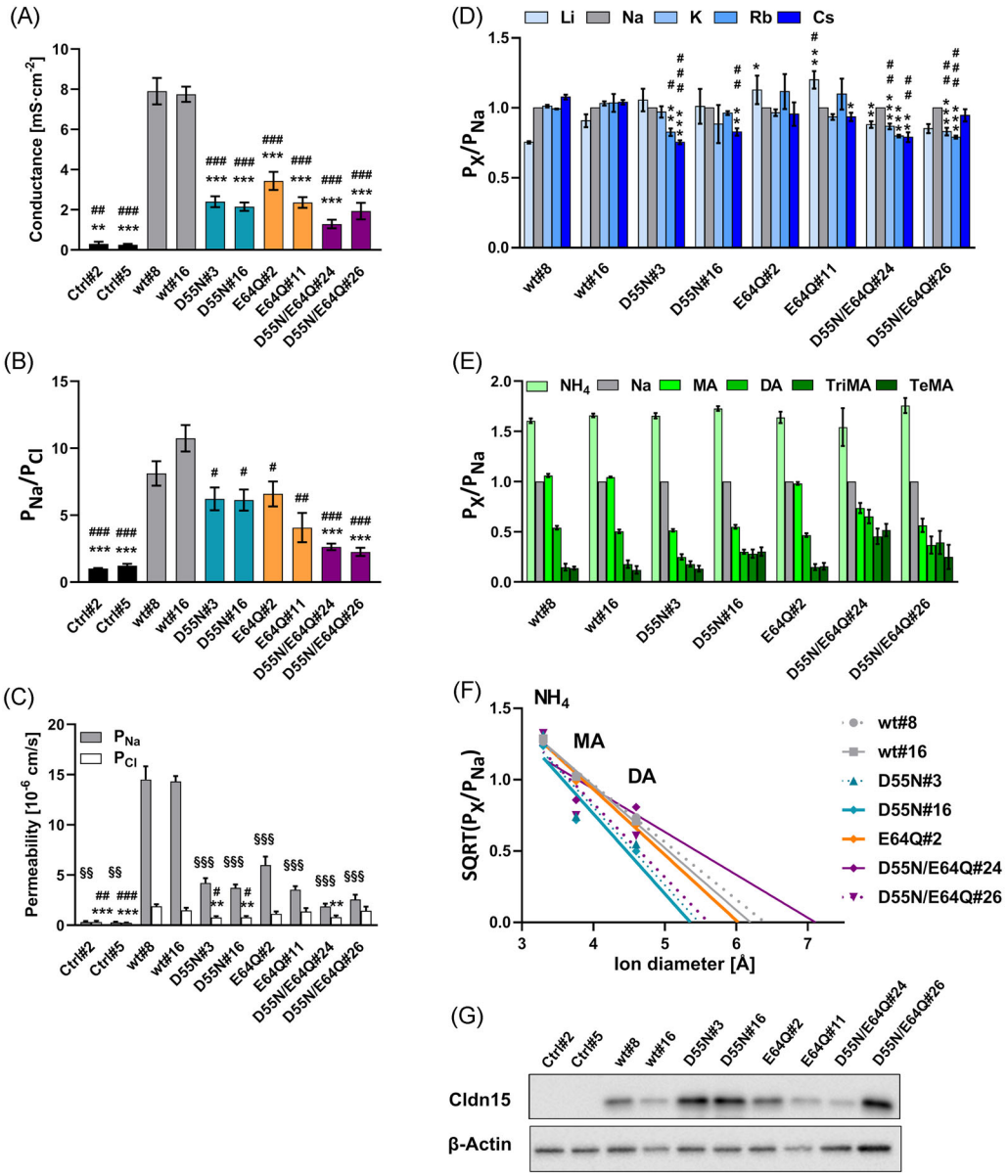

FIGURE 3 Ion permeability of MDCK-C7 cell monolayers expressing Cldn15-D55N, -E64Q, or -D55N/E64Q. (A) TER measurements showed that Cldn15-mediated conductance (1/TER) was similarly decreased by D55N, E64Q, and D55N/E64Q ($n = 7–12$). (B) Dilution potentials showed that P_{Na}/P_{Cl} is moderately decreased by D55N and E64Q but more strongly decreased by D55N/E64Q ($n = 7–13$). (C) For D55N, E64Q, and D55N/E64Q, P_{Na} was decreased more strongly than P_{Cl} ($n = 7–13$). (D) While for Cldn15-wt, permeability for alkali metal cations increased with unhydrated ion radius (Eisenman I, II), it decreased with unhydrated ion radius for D55N (Eisenman X, XI). Also, for E64Q and D55N/E64Q, the Eisenman sequence was altered ($n = 3–14$). (E) Relative permeabilities for NH_4, methylammonium (MA), dimethylammonium (DA), trimethylammonium (TriMA), and tetramethylammonium (TeMA). (F) Applying Renkin equation indicated smaller pore diameter for Cldn15-D55N. (G) Expression levels of Cldn15 constructs in stable MDCK-C7 clones. $^{*, **, ***}$ P_{Cl} versus wt#8; $^{\#, \#\#, \#\#\#}$ P_{Cl} versus wt#16; $^{§§, §§§}$ P_{Na} versus wt#8 and wt#16 (significance identical for testing against wt#8 or wt#16)

Cldn15-W63K shows ion permeability properties largely similar to that of Cldn15-wt

Similar to Cldn15-wt-expressing MDCK-C7 lines, Cldn15-W63K-expressing lines showed a much higher conductance than vector control monolayers (Figure 5A). The conductances for Cldn15-W63K lines were in between those of Cldn15-wt#2/–wt#27 lines, which were generated in parallel, and those of other Cldn15-wt lines generated earlier (Figure 3A). P_{Na}/P_{Cl} was very similar for Cldn15-W63K and Cldn15-wt (Figure 5B). In addition, the relative permeabilities to alkali metal cations (Figure 5C,D) and organic cations (Figure 5E,F) were similar for Cldn15-W63K and Cldn15-wt. Just a slightly lower P_{Li}/P_{Na} and P_{Cs}/P_{Na} was observed for Cldn15-W63K (Eisenman sequence IV = > V). The pore diameter was assessed to be similar

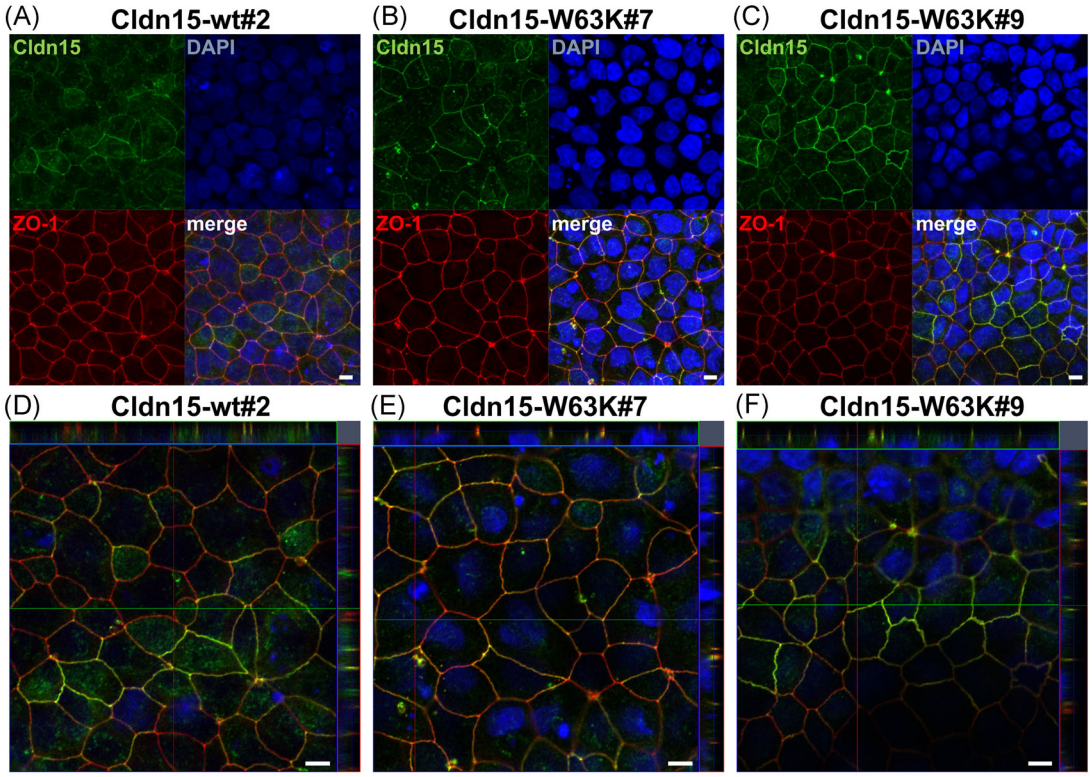

FIGURE 4 (A–F) In MDCK-C7 cells, Cldn15-W63K localized to the TJ as indicated by colocalization with the TJ marker ZO-1 in the apicolateral plasma membrane, similar to Cldn15-wt. Immunostaining, confocal z-stacks; bar, 5 μm. (A–C) Maximum projection, split channels. (D–F) Orthoscopic view, merge. #Monoclonal line number

(Cldn15-wt: ~5.9 Å and Cldn15-W63K: ~5.7/5.8 Å). Finally, P_{Ca}/P_{Na} was found to be similar for Cldn15-wt, Cldn15-W63K, and Cldn10b-wt (Figure 5G).

Together, the data indicate that W63K does neither significantly change charge selectivity and ion dehydration capability nor pore size of the Cldn15 channel.

K64M and K64W substitutions disturb the integration of Cldn10b into TJs

For the purpose of comparison with the Cldn10b-mimicking Cldn15-W63K, the complementary Cldn15-mimicking substitution was analyzed in Cldn10b (K64W). In addition, the charge-removing substitution K64M was analyzed in Cldn10b.

In contrast to Cldn15-W63K, Cldn10b-K64W was not capable to form wt-like TJ strands in the HEK cell reconstitutions system (Figure S3). A similar disturbance of TJ strand formation was previously shown for Cldn10b-K64M.[17] This indicated that in Cldn10b, the positive charge of K64 supports assembly into homopolymeric strands, whereas in Cldn15, a positive charge at the corresponding position does not influence assembly into homopolymeric strands.

In MDCK-C7 cells, Cldn10b-K64W and Cldn10b-K64M were detected in the occludin-positive apicolateral TJ domain of the plasma membrane, however, to a much lesser extent than Cldn10b-wt (Figure 6). In strong contrast to Cldn10b-wt, the mutants were largely detected along the whole lateral membrane. Together with the freeze fracture data (Figure S3), this indicates that self- and coassembly with other TJ proteins was altered for Cldn10b-K64W and Cldn10b-K64M, but that still a fraction of these mutants was integrated into endogenous TJs. Thus, in contrast to the corresponding position in Cldn15 (63), the charge at position 64 in Cldn10b does strongly influence TJ integration.

K64M and K64W substitution increase permeability of Cldn10b channels for monovalent cations larger than sodium but smaller than trimethylammonium cations

The expression of Cldn10b-wt strongly increased conductance and P_{Na}/P_{Cl} of MDCK-C7 monolayers (Figure 7B,C), similar to previous studies.[17,24] In addition, the expression of Cldn10b-K64W and -K64M increased conductance and P_{Na}/P_{Cl}. However, the extent of these effects varied strongly between the different lines. Whereas for Cldn10b-wt this mainly correlated with expression level, this was not clearly the case for the mutants (Figure 7A–C). For the mutants, most of Cldn10b is expected to reside outside of TJ and thus not to contribute to conductance (Figure 6). The variability between the mutant lines might potentially be related to varying integration of the mutant

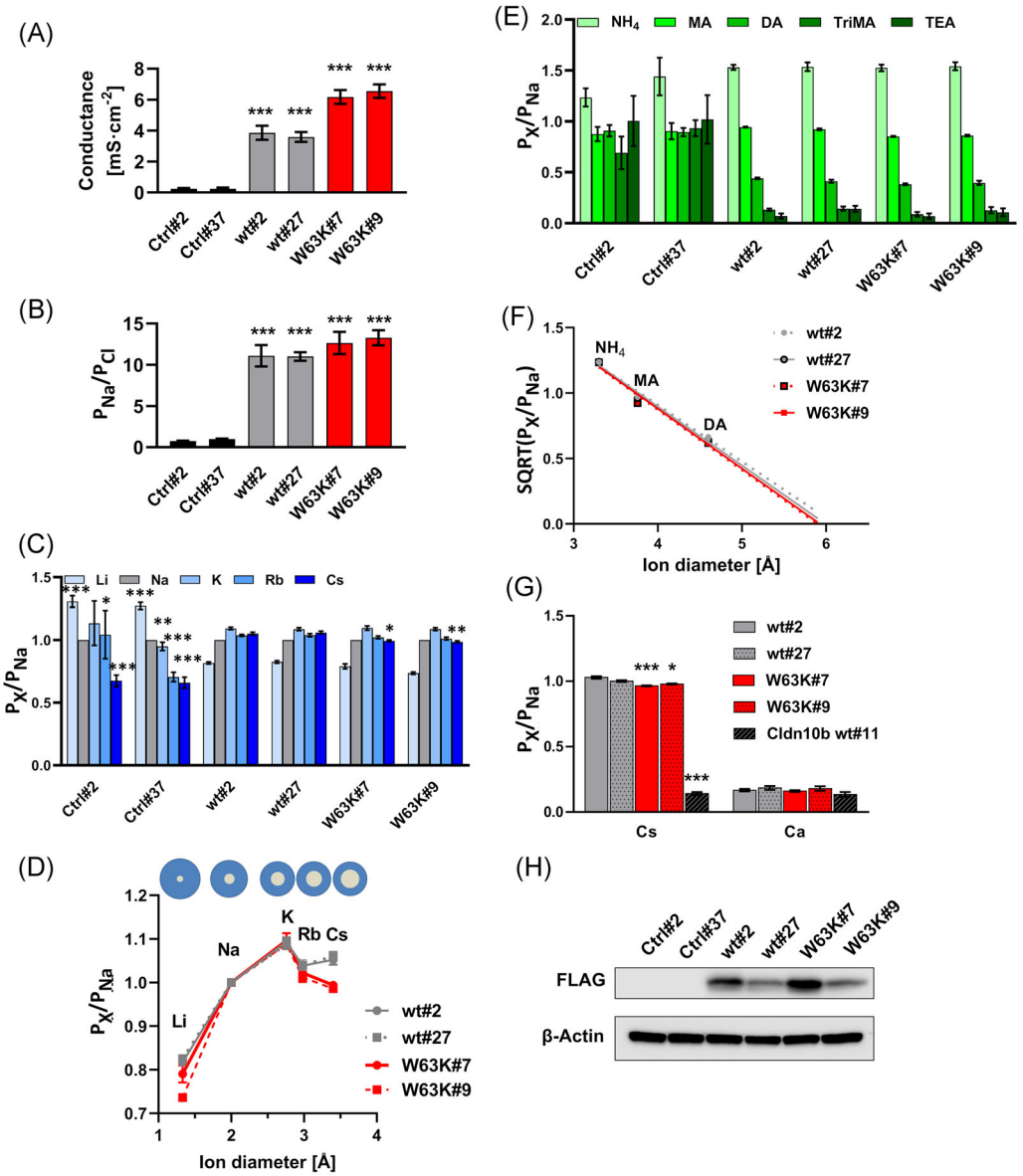

FIGURE 5 Cldn15-W63K forms wild-type-like cation channels. (A) Expression of Cldn15-wt and -W63K strongly increased conductance ($n = 8–16$). Ctrl#2 not identical with Ctrl#2 of Figure 3. (B) W63K mutation did not affect P_{Na}/P_{Cl} ($n = 8–16$). A, B—tested versus Ctrl#2. (C, D) W63K mutation only slightly changed alkali metal ion permeability, indicated by marginally decreased P_{Li}/P_{Na} and P_{Cs}/P_{Na}. The resulting Eisenman sequences changed from IV to V. Size of ions with hydration shells is illustrated at top in D ($n = 6–15$). (E) Biionic potentials also indicated similar permeabilities for organic cations in Cldn15-wt and Cldn15-W63K ($n = 6–10$). (F) Applying the Renkin equation yielded similar pore diameters for Cldn15-wt and -W63K. (G) Cldn15-W63K showed a low P_{Ca}/P_{Na} similar to that of Cldn15-wt and Cldn10b-wt. P_{Cs}/P_{Na} known to differ between Cldn15-wt and Cldn10b-wt is shown for comparison ($n = 3–6$). C, G—tested versus wt#2. (H) Western blot showed differences in expression level between Cldn15 lines; however, these did not correlate with above-mentioned functional parameters. #Monoclonal line number, with the exception of polyclonal pool Cldn10b-wt#11 in (G). Abbreviations: DA, dimethylammonium; MA, methylammonium; TEA, triethylammonium; TriMA, trimethylammonium

channels into endogenous TJs. In addition, the altered assembly properties of the mutants (Figure S3) might disturb the nonselective barrier formed by endogenous TJ strands slightly differently in the individual lines. Nevertheless, at least one mutant line (Cldn10b-K64M#2) showed a conductance and P_{Na}/P_{Cl} similar to that of Cldn10b-wt (Figure 7B,C). This demonstrated that the positive charge of K64 is not essential for the formation of cation-selective Cldn10b channels.

Biionic potential measurements resulted in the same Eisenman sequence (X) for Cldn10b-wt, -K64W, and -K64M. However, for the mutant lines, P_K/P_{Na}, P_{Rb}/P_{Na}, and P_{Cs}/P_{Na} were slightly higher than those for Cldn10b-wt (Figure 7D and Figure S4A). This indicated that the K64W and K64M substitutions slightly weaken the ion dehydration capability of Cldn10b channels.

In addition, compared to Cldn10b-wt, for the mutant lines, a considerably higher and more Cldn15-like relative permeability for NH_4 (P_{NH4}/P_{Na}) was obtained. In addition, higher P_X/P_{Na} were obtained for methylammonium and at least for Cldn10b-K64M#2 also for dimethylammonium cations (Figure 7E and Figure S4B). Due to the very

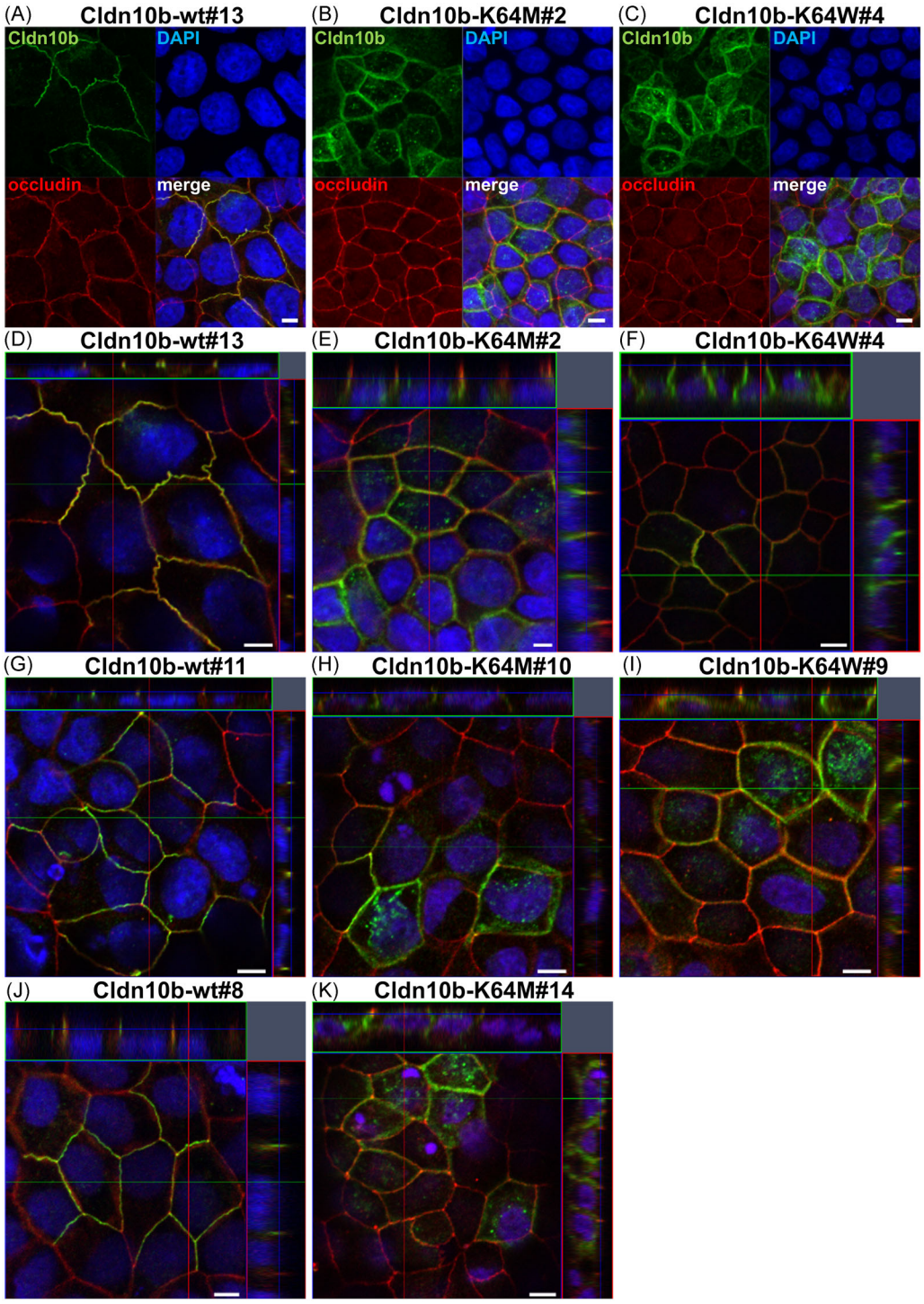

FIGURE 6 Cldn10b-K64M and Cldn10b-K64W localized only partly to TJs of MDCK-C7 cells. Immunostaining, confocal z-stacks; bar, 5 μm; #polyclonal pool number. (A, D, G, J) Cldn10b-wt was largely restricted to the occludin-positive TJ domain in apicolateral plasma membrane. (B, E, H, K) Only a fraction of Cldn10b-K64M localized to occludin-positive TJ, most was spread along lateral membrane. (C, F, I) Only a fraction of Cldn10b-K64W localized to occludin-positive TJ, most was spread along lateral membrane. Maximum projection, split channels (A–C); orthoscopic views, merge (D–K)

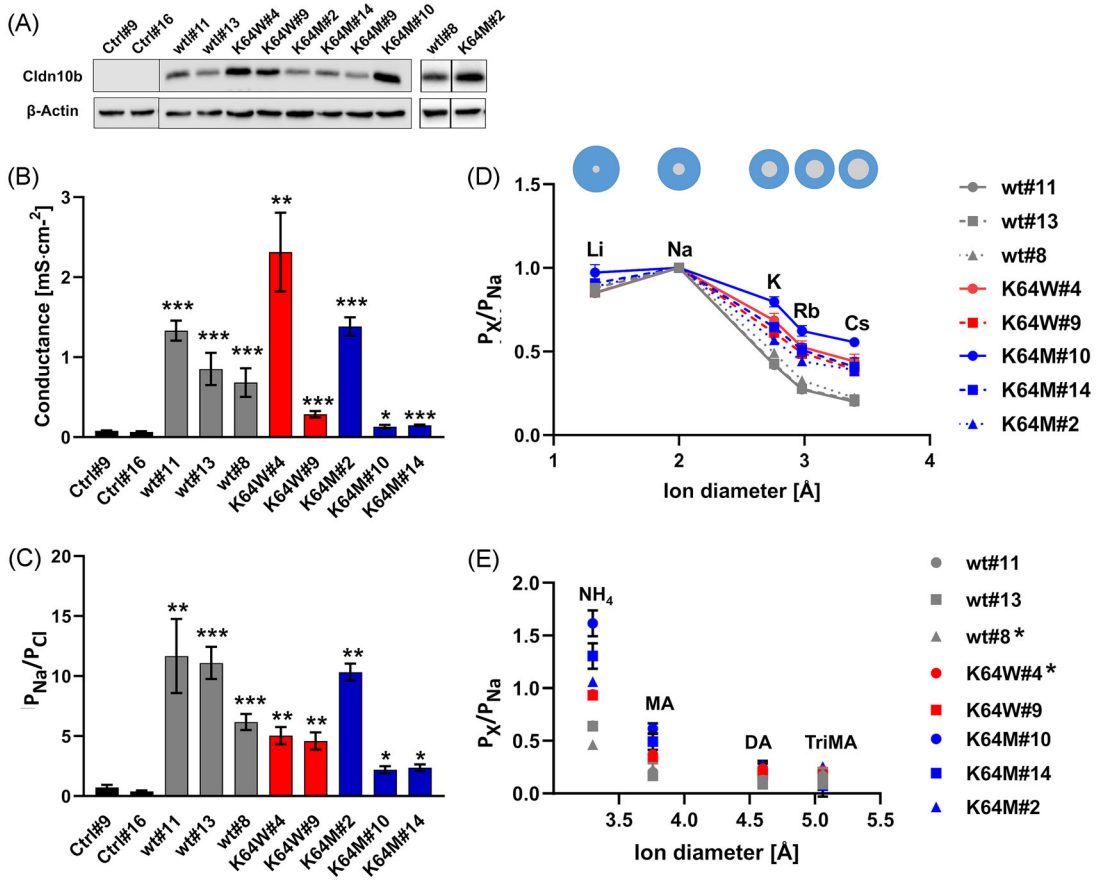

FIGURE 7 Ion permeability of MDCK-C7 cell monolayers stably expressing Cldn10b-wt, Cldn10b-K64W, or Cldn10b-K64M. (A) Cldn10b expression levels differed to some extent between polyclonal lines analyzed. (B) All Cldn10b-expressing lines showed higher conductance than control monolayers. The conductance differed strongly between the lines ($n = 6–14$). (C) All Cldn10b-expressing lines showed higher P_{Na}/P_{Cl} than controls. P_{Na}/P_{Cl} differed strongly between the lines ($n = 6–15$). (D) Compared to Cldn10b-wt–expressing monolayers, those expressing Cldn10b-K64W or -K64M showed similar Eisenman sequence (X), albeit with higher P_K/P_{Na}, P_{Rb}/P_{Na}, and P_{Cs}/P_{Na} ($n = 5–15$). (E) All mutant lines showed higher P_X/P_{Na} for NH_4 and methylammonium (MA) than Cldn10b-wt, and Cldn10b-K64M#2 also for dimethylammonium (DA) cations ($n = 4–14$). [#]polyclonal line number. Significance was tested versus Ctrl#9. Abbreviation: TriMA, trimethylammonium

similar relative permeabilities for methylammonium, dimethylammonium, and trimethylammonium ions, linear regression for calculation of the pore size was hindered. Nevertheless, the data indicate that the cutoff size for ion permeation through Cldn10b channels is in the range of dimethylammonium ions (4.6 Å) and that K64W and K64M slightly widen the pore and increase permeability for NH_4 cations.

Cldn10b-D36A is integrated into TJs in a Cldn10b-wt–like manner

In contrast to the other cation channel-forming TJ proteins Cldn2 and Cldn15, Cldn10b contains a negatively charged residue (D36) in the β1β2-loop of the ECS1 (Figure 1B,D). Alignments of Cldn10b-like sequences of vertebrates revealed that the presence of an aspartate at this position correlates very strongly with the presence of a positive charge at the position corresponding to K64 in human Cldn10b. Furthermore, the corresponding neighboring residue in human Cldn10a (R33) was shown to be involved in anion selectivity.[12] Thus, to investigate the role of D36 in the Cldn10b channel, the substitution D36A was investigated. Previously, we showed that the expression of Cldn10b-D36A in HEK cells reconstitutes wt-like TJ strands.[17] Stable expression of Cldn10b-D36A in MDCK-C7 cells led to prominent integration of Cldn10b-D36A into endogenous TJs, similar as found for Cldn10b-wt (Figure S5). Thus, in contrast to K64W and K64M, the D36A substitution does not alter strand formation and TJ integration of Cldn10b.

D36A substitution does not change ion channel properties of Cldn10b

Similar to Cldn10b-wt-expressing MDCK-C7 lines, Cldn10b-D36A-expressing lines showed higher conductance (Figure 8B) and higher P_{Na}/P_{Cl} (Figure 8C) than control monolayers. For Cldn10b-D36A#5, conductance and P_{Na}/P_{Cl} were much higher than for Cldn10b-wt. However, for Cldn10b-D36A#13, conductance and P_{Na}/P_{Cl} were lower than for Cldn10b-wt. This variability between the Cldn10b-D36A lines correlated with the Cldn10b expression level/rate (Figure 8A–C).

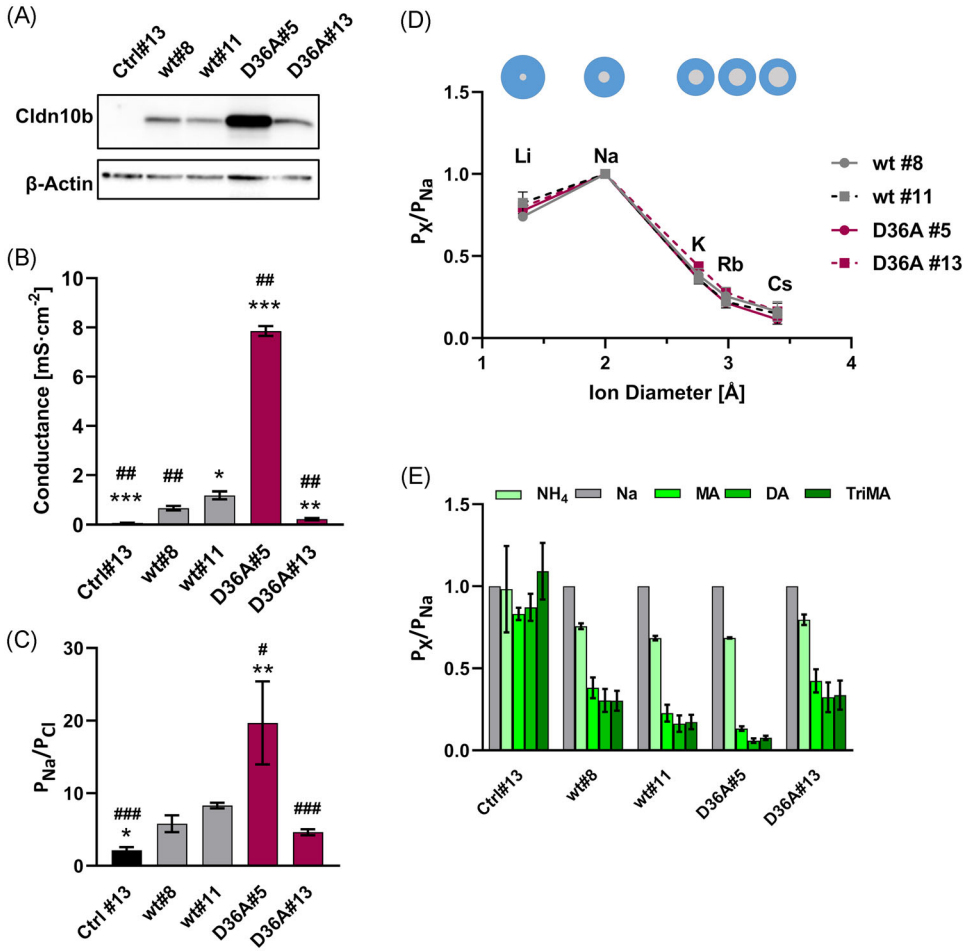

FIGURE 8 Cldn10b-D36A forms wild-type-like cation channels. MDCK-C7 polyclonal lines expressing Cldn10b-D36A or Cldn10b-wt. (A) Western blot showing differences in expression level between Cldn10b-D36A#5 and Cldn10b-D36A#13. (B) Conductance was higher for all Cldn10b-expressing lines than for controls (Ctrl#13). Conductance differed between lines and correlated with Cldn10b expression level. TER measurements ($n = 6–8$). (C) P_{Na}/P_{Cl} was higher for all Cldn10b-expressing lines than for controls. P_{Na}/P_{Cl} differed between lines and correlated with Cldn10b expression level ($n = 6–8$). (D) For Cldn10b-D36A, P_{Li}/P_{Na}, P_K/P_{Na}, P_{Rb}/P_{Na}, P_{Cs}/P_{Na}, and Eisenman sequences were similar to those for Cldn10-wt ($n = 5–9$). Size of ions with hydration shells is illustrated at top. (E) For Cldn10b-D36A, P_{NH4}/P_{Na}, P_{MA}/P_{Na}, P_{DA}/P_{Na}, and P_{TriMA}/P_{Na} were similar to those for Cldn10b-wt ($n = 6–9$). Linear regression analysis for estimation of pore size was hindered by very similar absolute permeabilities for MA, DA, and TriMA, which all were in the range of control. $n = 6–8$, *, **, *** versus wt#8; $^{\#}$, $^{\#\#}$, $^{\#\#\#}$ versus wt#11. Abbreviations: DA, dimethylammonium; MA, methylammonium; TriMA, trimethylammonium

The relative permeabilities to alkali metal cations (Figure 8D) and monovalent organic cations (Figure 8E) for Cldn10b-D36A were similar to those for Cldn10b-wt. Minor differences, for instance, in P_{MA}/P_{Na}, P_{DA}/P_{Na}, and P_{TriMA}/P_{Na}, were rather related to different Cldn10b-D36A expression levels. In sum, the data indicate that the negative charge of D36 residue is not critically involved in determination of charge and size selectivity, as well as ion dehydration pattern of Cldn10b channels.

DISCUSSION

In this study, we analyzed the role of charged pore-lining residues in Cldn10b and Cldn15 cation channels (see Table S2 for a summary). Charge-neutralizing mutations D55N and E64Q reduced ion conductance and charge selectivity of Cldn15 channels. In addition, D55N decreased the pore diameter and strongly shifted the Eisenman sequence. W63K in Cldn15 had no effect, whereas the corresponding K64W in Cldn10b strongly disturbed TJ integration. The results indicate common and different mechanistic aspects of Cldn10b and Cldn15 cation channels.

Previous studies have shown that the cation channels formed by Cldn15, −10b, and −2 share high permeability for monovalent over divalent cations but differ in pore size and ion dehydration pattern.[5,13,22,24] Cldn15 prefers larger over smaller alkali metal cations (Eisenman sequence I–IV). For Cldn10b, this is approximately contrariwise (Eisenman sequence X/XI) and for Cldn2, it is close to that of Cldn10b (Eisenman sequence IX). This indicates that cation dehydration within the channel increases in the order Cldn15 < Cldn2 < Cldn10b. Furthermore, in contrast to

Cldn15 and Cldn2 channels, Cldn10b channels are largely water impermeable.[22,23]

To assess the contribution of charged pore-lining residues on these properties of Cldn15 and Cldn10b channels, we electrophysiologically compared wild-type claudins with the respective mutants stably expressed in tight MDCK-C7 cells. For Cldn10b-wt and Cldn15-wt, charge selectivity (P_{Na}/P_{Cl}), Eisenman sequence (P_x/P_{Na} for alkali metal cations), and pore size (P_x/P_{Na} for organic cations) were similar to previous studies.[22,24]

The neutralizing mutations D55N and E64Q of charged residues that are conserved between Cldn15 and Cldn10b did not alter the integration of Cldn15 into endogenous TJs of MDCK-C7 cells (Figure 2). However, they reduced ion conductance of Cldn15 channels strongly, whereas charge selectivity was less affected. In other words, the mutations reduced sodium permeability and to a lesser extent also chloride permeability (Figure 3A–C). Thus, the negative charges of D55 and E64 do not only contribute to the selective attraction of cation and barrier for anions but also to solute permeation in general. The latter could be due to effects on the pore shape. D55N decreased pore diameter and strongly shifted the Eisenman sequence, indicating increased ion dehydration capability of the pore (Figure 3D–F). E64Q had less clear effects and D55N/E64Q double mutation had an additive effect on charge selectivity but a rather counteracting effect on relative monovalent cation permeabilities. This indicates that D55 and E64 contribute to channel properties by at least partly different mechanisms that might include the following: According to the models of the Cldn15/Cldn10b channel structure, D55/D56 from four chains are collectively oriented to the pore center, where they likely interact with the permeating cation. In contrast, E64/D65 is located at the pore rim and may at least partly shielded by residues, such as W63/K64 (Figure 1B,C and Figure S6). This shielding is supported by the finding that the positive charge of K64 in Cldn10b and that of K63 in Cldn15-W63K (that potentially interacts with E64/D65) does not interfere with cation selectivity of the channels (Figures 5B and 7).

Strikingly, compared to the strong shift in Eisenman sequence from I–IV to X/XI caused by D55N in Cldn15, the opposite was found for D65N (ion interaction site-neutralizing mutation) in Cldn2 cation channels: For Cldn2-D65N, the Eisenman sequence (IX) was not changed and P_{Li}/P_{Na} was not increased but decreased.[13] This indicates that the negative charges in the pore center regulate cation dehydration and selectivity in Cldn15 and Cldn2 channels differently.

That Cldn15 and Cldn10b differ in some channel properties is likely due to differing residues in ECS1, since the latter has been shown to determine permeability properties of the claudin channels.[9,26] According to the Cldn10b and Cldn15 channel models (Figure 1),[17] the following 13 pore-lining ECS1 residues differ between Cldn10b and Cldn15 (at least for human and mouse): K31/R30, I35/V34, D36/H35, T38/N37, A43/N42, Y45/I44, A47/E46, A52/S51, V54/A53, T58/L57, K64/W63, D65/E64, and D73/S72.

We here focused on the differences of D36 versus H35 and K64 versus W63 because they strongly correlate for Cldn10b/Cldn15-like sequences of different vertebrate species. Neither D36A, K64W, or K64M in Cldn10b nor W63K in Cldn15 led to a major shift in Eisenman sequence (Figures 5, 7, and 8). Nevertheless, Cldn10b-K64M and -K64W showed a somewhat more Cldn15-like NH_4^+- and alkali metal cation permeability than Cldn10b-wt (Figure 7 and Figure S4). Preliminary measurements did not indicate a clear effect of Cldn10b/15 chimeric mutations on water permeability (data not shown). Thus, the presence of D36 or K64 alone seems not to be essential for Cldn10b-like permeability properties, even though K64 contributes to the latter. Nevertheless, we speculate that the differing patterns between Cldn10b and −15 of hydrophilic and hydrophobic residues close to the pore center (indicated by the structural models) contribute to the lower ion dehydration capability, larger pore size, and higher water permeability of Cldn15 channels.[22,23]

D73/S72 is located at the pore entrance, and thus, unlikely affects selectivity. K31/R30 does not change the charge and is not located in the pore center. I35/V34 and V44/A43 do not change electrostatic properties. MDCK cell lines expressing Cldn15-mimicking Cldn10b-A47E/A52S did not provide reliable results so far (data not shown). Thus, further studies should also include the remaining differing residues T38/N37, A43/N42, Y45/I44, and T58/L57.

Interestingly, Cldn15-D55N preferred smaller over larger alkali metal cation (Eisenman sequence X/XI), approximately similar to Cldn10b (Eisenman sequence X/XI) (Figures 3D and 7D). However, the Eisenman sequence cannot be mainly determined by a negative charge at this position since it is conserved between Cldn15 and Cldn10b. This indicates that D55/D56 together with other residues lining the pore close to the center determine the dehydration patterns of Cldn10b and Cldn15 channels.

The result that D55N in Cldn15 decreases pore diameter (Figure 3F) indicates that charge repulsion in the region of the proposed central ring of four D55 residues (Figure 1C)[16,17] contributes to shape of the pore at its narrowest site. Despite the conservation of D55/D56 between Cldn15 and Cldn10b, the pore diameter was estimated to be smaller for the latter ($\leq$ 5.2 Å for Cldn10b vs. $\geq$ 6.0 Å for Cldn15; Figures 3 and 7).[22] Therefore, and according to the channel models reported previously,[11,16,17] we propose that the extent of the central repulsion differs between Cldn10b and Cldn15 due to different electrostatic potential, flexibility, and interaction pattern of residues close to the tetra-D55/D56 ring. The claudin octamer models (Figure 1) possess pore diameters at the most constricted part of ∼4.3 Å for Cldn10b and ∼5.2 Å for Cldn15. These values differ from the above-mentioned experimentally determined ones to a certain extent. Nevertheless, the tendency toward a smaller pore diameter for Cldn10b is given in the models. However, further studies, for instance, using molecular dynamics simulations with different model variants of oligomeric claudin channels, have to be performed to validate, refine, and improve the models. In addition, further experimental studies are needed. For instance, it would be of interest to compare Cldn15-D55N and Cldn10b-D56N with respect to effects on conductance, P_{Na}/P_{Cl}, relative permeabilities of the different alkali metal ions, and pore size.

The Cldn10b-mimicking W63K substitution in Cldn15 did not affect strand formation in HEK cells and integration into endogenous TJs, charge selectivity, dehydration capability, or pore size of the Cldn15 channel in MDCK-C7 cells (Figure S3, Figures 4 and 5). In contrast,

the corresponding Cldn15-mimicking K64W and charge-neutralizing K64M in Cldn10b strongly disturbed strand formation and integration of Cldn10b into TJs (Figure S3 and Figure 6). In addition, K64M/K64W slightly weakened ion dehydration capability and slightly increased the diameter of Cldn10b pores (Figure 7D,E). Thus, a positive charge at position 63/64 close to the pore center affects Cldn15 and Cldn10b channels differently. It appears to selectively stabilize homopolymerization and heteropolymerization with endogenous TJ proteins for Cldn10b. This implies that position 63/64 is close to an interchain interface that differs between Cldn10b and Cldn15. According to the oligomeric channel models and depending on its orientation, this position could contribute to the *face-to-face-cis*-, *linear-cis*-, and *cis*- or *trans*-interface with the ECS1-β1β2 loop (Figure 1).[11,17] However, the mechanistic and structural base for claudin homo- and hetero-oligomerization is unclear in detail. Some patterns of claudin hetero-compatibility and some involved protein regions are known.[2,27–29] For instance, in contrast to Cldn1 to −5, for Cldn10b, only homo- but no hetero-oligomerization with other claudins has been observed. Nevertheless, Cldn10b as well as Cldn15 channels copolymerize in MDCK-C7 cells with endogenous TJ proteins that include Cldn1, −3, −4, −5, −7, −8, and occludin to form a continuous barrier for solutes other than small cations.[22,24] Thus, the selective disturbance in Cldn10b assembly caused by K64W/K64M might contribute to the molecular understanding of TJ stand assembly in general.

As mentioned above, the presence of the negatively charged D36 strongly correlates with the presence of a positive charge at position 64 (K64) for Cldn10b/Cldn15-like sequences of different vertebrate species. In addition, in the model of the Cldn10b oligomeric channel, K64 and D36 of neighboring protomers (chains) are in close proximity to each other. However, in contrast to charge removal of K64 (K64W and K64M), opposite charge removal by D36A did not have any effect on strand formation, TJ integration, or function of Cldn10b channels (Figure S5 and Figure 8). This suggests that assembly and ion selectivity of Cldn10b channels do not depend on electrostatic interaction between K64 and D36.

In summary, this structure-function study compared Cldn15 and −10b cation channels by functional mapping of pore-lining residues. In Cldn15, D55N and E64Q decreased ion permeability more strongly than charge selectivity. D55N increased cation dehydration capability and decreased pore diameter. Charge at position W63/K64 affects the assembly of Cldn15 and Cldn10b channels differently. In addition, W63/K64 is proposed to shield E64/D65 at least partly, whereas D55/D56 in the pore center of claudin-15/−10b channels directly attracts cations. It is plausible that further cell biological, electrophysiological, and molecular dynamics simulation-based comparison of Cldn10b and Cldn15 channels will shed light on further mechanistic details. Thus, our present study provides one further step on the way to full elucidation of the molecular determinants of paracellular cation permeability.

ACKNOWLEDGMENTS

This research was funded by the Deutsche Forschungsgemeinschaft (DFG PI 837/4-1 and 4-2; DFG FR 652/12-1, DFG GU 447/14-1 and 14-2, GRK 2318), the Charité – Universitätsmedizin Berlin (Promotionsabschlussstipendium for Caroline Hempel), and Sonnenfeld Stiftung, Berlin (funding of equipment). We thank In-Fah Lee and Britta Jebautzke for their expert technical assistance and Dr. Santhosh Kumar Nagarajan for useful discussions.

Open access funding enabled and organized by Projekt DEAL.

COMPETING INTERESTS

The authors declare that they have no competing interests.

AUTHOR CONTRIBUTIONS

C.H. and D.G.: acquisition of data, analysis and interpretation of data, participated in drafting the manuscript or revising its intellectual content. R.R. and J.P.: conception and design, acquisition of data, analysis and interpretation of data, participated in drafting the manuscript or revising its intellectual content. A.F.: acquisition of data, analysis and interpretation of data, and participated in drafting the manuscript. S.M.K.: analysis and interpretation of data, participated in drafting and revising the manuscript. M.F.: conception and design, interpretation of data, participated in drafting the manuscript or revising its intellectual content.

ORCID

Caroline Hempel https://orcid.org/0000-0003-0347-5813
Rita Rosenthal https://orcid.org/0000-0002-5807-9415
Anja Fromm https://orcid.org/0000-0003-4091-9612
Susanne M. Krug https://orcid.org/0000-0002-1293-2484
Michael Fromm https://orcid.org/0000-0003-4497-7983
Dorothee Günzel https://orcid.org/0000-0002-7998-7164
Jörg Piontek https://orcid.org/0000-0002-0880-8915

REFERENCES

1. Günzel, D., & Fromm, M. (2012). Claudins and other tight junction proteins. *Comprehensive Physiology*, *2*, 1819–1852.
2. Piontek, J., Krug, S. M., Protze, J., Krause, G., & Fromm, M. (2020). Molecular architecture and assembly of the tight junction backbone. *Biochimica et Biophysica Acta Biomembranes*, *1862*, 183279.
3. Klar, J., Piontek, J., Milatz, S., Tariq, M., Jameel, M., Breiderhoff, T., Schuster, J., Fatima, A., Asif, M., Sher, M., Mäbert, K., Fromm, A., Baig, S. M., Günzel, D., & Dahl, N. (2017). Altered paracellular cation permeability due to a rare CLDN10B variant causes anhidrosis and kidney damage. *PLoS Genetics*, *13*, e1006897.
4. Sewerin, S., Piontek, J., Schönauer, R., Grunewald, S., Rauch, A., Neuber, S., Bergmann, C., Günzel, D., & Halbritter, J. (in press). Defective claudin-10 causes a novel variation of HELIX syndrome through compromised tight junction strand assembly. *Genes and Diseases*, https://doi.org/10.1016/j.gendis.2021.06.006.
5. Günzel, D., & Yu, A. S. L. (2013). Claudins and the modulation of tight junction permeability. *Physiological Reviews*, *93*, 525–569.
6. Suzuki, H., Tani, K., Tamura, A., Tsukita, S., & Fujiyoshi, Y. (2015). Model for the architecture of claudin-based paracellular ion channels through tight junctions. *Journal of Molecular Biology*, *427*, 291–297.
7. Colegio, O. R., Van Itallie, C. M., Mccrea, H. J., Rahner, C., & Anderson, J. M. (2002). Claudins create charge-selective channels in the paracellular pathway between epithelial cells. *American Journal of Physiology-Cell Physiology*, *283*, C142–C147.
8. Conrad, M. P., Piontek, J., Günzel, D., Fromm, M., & Krug, S. M. (2016). Molecular basis of claudin-17 anion selectivity. *Cellular and Molecular Life Sciences*, *73*, 185–200.

9. Krause, G., Protze, J., & Piontek, J. (2015). Assembly and function of claudins: Structure–function relationships based on homology models and crystal structures. *Seminars in Cell & Developmental Biology*, *42*, 3–12.
10. Li, J., Zhuo, M., Pei, L., Rajagopal, M., & Yu, A. S. L. (2014). Comprehensive cysteine-scanning mutagenesis reveals claudin-2 pore-lining residues with different intrapore locations. *Journal of Biological Chemistry*, *289*, 6475–6484.
11. Samanta, P., Wang, Y., Fuladi, S., Zou, J., Li, Ye, Shen, Le, Weber, C., & Khalili-Araghi, F. (2018). Molecular determination of claudin-15 organization and channel selectivity. *Journal of General Physiology*, *150*, 949–968.
12. Van Itallie, C. M., Rogan, S., Yu, A., Vidal, L. S., Holmes, J., & Anderson, J. M. (2006). Two splice variants of claudin-10 in the kidney create paracellular pores with different ion selectivities. *American Journal of Physiology - Renal Physiology*, *291*, F1288–F1299.
13. Yu, A. S. L., Cheng, M. H., Angelow, S., Günzel, D., Kanzawa, S. A., Schneeberger, E. E., Fromm, M., & Coalson, R. D. (2009). Molecular basis for cation selectivity in claudin-2-based paracellular pores: Identification of an electrostatic interaction site. *Journal of General Physiology*, *133*, 111–127.
14. Suzuki, H., Nishizawa, T., Tani, K., Yamazaki, Y., Tamura, A., Ishitani, R., Dohmae, N., Tsukita, S., Nureki, O., & Fujiyoshi, Y. (2014). Crystal structure of a claudin provides insight into the architecture of tight junctions. *Science*, *344*, 304–307.
15. Alberini, G., Benfenati, F., & Maragliano, L. (2017). A refined model of claudin-15 tight junction paracellular architecture by molecular dynamics simulations. *PLoS One*, *12*, e0184190.
16. Alberini, G., Benfenati, F., & Maragliano, L. (2018). Molecular dynamics simulations of ion selectivity in a claudin-15 paracellular channel. *Journal of Physical Chemistry B*, *122*, 10783–10792.
17. Hempel, C., Protze, J., Altun, E., Riebe, B., Piontek, A., Fromm, A., Lee, I. M., Saleh, T., Günzel, D., Krause, G., & Piontek, J. (2020). Assembly of tight junction strands: Claudin-10b and claudin-3 form homotetrameric building blocks that polymerise in a channel-independent manner. *Journal of Molecular Biology*, *432*, 2405–2427.
18. Irudayanathan, F. J., Wang, X., Wang, N., Willsey, S. R., Seddon, I. A., & Nangia, S. (2018). Self-assembly simulations of classic claudins—Insights into the pore structure, selectivity, and higher order complexes. *Journal of Physical Chemistry B*, *122*, 7463–7474.
19. Zhao, J., Krystofiak, E. S., Ballesteros, A., Cui, R., Van Itallie, C. M., Anderson, J. M., Fenollar-Ferrer, C., & Kachar, B. (2018). Multiple claudin–claudin cis interfaces are required for tight junction strand formation and inherent flexibility. *Communications Biology*, *1*, 50.
20. Nakamura, S., Irie, K., Tanaka, H., Nishikawa, K., Suzuki, H., Saitoh, Y., Tamura, A., Tsukita, S., & Fujiyoshi, Y. (2019). Morphologic determinant of tight junctions revealed by claudin-3 structures. *Nature Communications*, *10*, 816.
21. Krause, G., Winkler, L., Mueller, S. L., Haseloff, R. F., Piontek, J., & Blasig, I. E. (2008). Structure and function of claudins. *Biochimica et Biophysica Acta*, *1778*, 631–645.
22. Rosenthal, R., Günzel, D., Piontek, J., Krug, S. M., Ayala-Torres, C., Hempel, C., Theune, D., & Fromm, M. (2020). Claudin-15 forms a water channel through the tight junction with distinct function compared to claudin-2. *Acta Physiologica (Oxford)*, *228*, e13334.
23. Rosenthal, R., Milatz, S., Krug, S. M., Oelrich, B., Schulzke, J.-D., Amasheh, S., Günzel, D., & Fromm, M. (2010). Claudin-2, a component of the tight junction, forms a paracellular water channel. *Journal of Cell Science*, *123*, 1913–1921.
24. Günzel, D., Stuiver, M., Kausalya, P. J., Haisch, L., Krug, S. M., Rosenthal, R., Meij, I. C., Hunziker, W., Fromm, M., & Müller, D. (2009). Claudin-10 exists in six alternatively spliced isoforms that exhibit distinct localization and function. *Journal of Cell Science*, *122*, 1507–1517.
25. Piontek, J., Winkler, L., Wolburg, H., Müller, S. L., Zuleger, N., Piehl, C., Wiesner, B., Krause, G., & Blasig, I. E. (2008). Formation of tight junction: Determinants of homophilic interaction between classic claudins. *FASEB Journal*, *22*, 146–158.
26. Colegio, O. R., Itallie, C. V., Rahner, C., & Anderson, J. M. (2003). Claudin extracellular domains determine paracellular charge selectivity and resistance but not tight junction fibril architecture. *American Journal of Physiology-Cell Physiology*, *284*, C1346–C1354.
27. Furuse, M., Sasaki, H., & Tsukita, S. (1999). Manner of interaction of heterogeneous claudin species within and between tight junction strands. *Journal of Cell Biology*, *147*, 891–903.
28. Milatz, S., Piontek, J., Hempel, C., Meoli, L., Grohe, C., Fromm, A., Lee, I.-F. M., El-Athman, R., & Günzel, D. (2017). Tight junction strand formation by claudin-10 isoforms and claudin-10a/-10b chimeras. *Annals of the New York Academy of Sciences*, *1405*, 102–115.
29. Daugherty, B. L., Ward, C., Smith, T., Ritzenthaler, J. D., & Koval, M. (2007). Regulation of heterotypic claudin compatibility. *Journal of Biological Chemistry*, *282*, 30005–30013.

SUPPORTING INFORMATION

Additional supporting information can be found online in the Supporting Information section at the end of this article.

How to cite this article: Hempel, C., Rosenthal, R., Fromm, A., Krug, S. M., Fromm, M., Günzel, D., & Piontek, J. (2022). Tight junction channels claudin-10b and claudin-15: Functional mapping of pore-lining residues. *Ann NY Acad Sci*., *1515*, 129–142. https://doi.org/10.1111/nyas.14794